

# Least-squares reverse time migration: Inversion-based imaging toward true reflectivity

CHONG ZENG, SHUQIAN DONG, and BIN WANG, TGS-NOPEC Geophysical Company

## Abstract

As an inversion-based imaging algorithm, least-squares reverse time migration (LSRTM) refines seismic images toward true-reflectivity earth models. It overcomes the shortcomings of conventional migration algorithms via iterative least-squares inversion to gradually correct migration errors. LSRTM also suppresses side lobes of image wavelets to generate images with high spatial resolution. Recovered weak events and steep dips are enhanced during iterations with balanced illumination. The true-amplitude behavior of LSRTM will greatly benefit quantitative seismic interpretations. LSRTM can be a practical image-domain broadband solution to generate high-resolution images with fine layers as well as accurate complex structures.

## Introduction

Exploration for hydrocarbons in various environments has pushed seismic-imaging techniques to evolve continuously in the past decades. The ultimate goal of seismic imaging is to provide a subsurface reflectivity model that accurately delineates underground structures with reliable physical attributes for geologic interpretation. Conventional depth-migration algorithms produce seismic images by extrapolating the source and receiver wavefields and applying imaging conditions. The inconsistency between the ideal imaging principle and the complicated real physics implies that there are always differences between a migration output and the true earth model. Because the difference is unavoidable, a natural way to minimize it is to introduce a geophysical inversion to refine the migration image toward the true reflectivity.

Building on the success of full-waveform inversion (FWI) for velocity model building, we can also apply iterative data-fitting-based inversion to seismic imaging. Pioneer researchers (e.g., Schuster, 1993; Nemeth et al., 1999) propose various inversion-based imaging algorithms to deal with the shortcomings of conventional seismic imaging. Nemeth et al. (1999) present a least-squares inversion approach to suppress the Kirchhoff migration artifacts from incomplete surface data.

More recently, least-squares solutions based on reverse time migration (RTM) (e.g., Dong et al., 2012; Wang et al., 2013; Dong et al., 2014) have been introduced to suppress the artifacts and improve the amplitude behavior of RTM images for real data.

Compared with the conventional migration algorithms that directly apply the imaging condition, the inversion-based imaging method refines depth images through least-squares inversion. Therefore, it is named least-squares migration (LSM). LSM usually consists of multiple steps of conventional migration and demigration. Because of the nature of multiple iterations, LSM has the major advantage that it can

gradually fix the errors introduced by the initial migration resulting from theoretical or implemental limitations.

Particularly when we use RTM as the migration and demigration engine for LSM, the method is called least-squares reverse time migration (LSRTM). LSRTM uses the two-way wave equation to image steep dips and complex structures. It inherits the advantages of general LSM and refines the RTM image toward true reflectivity for accurate structure locations as well as amplitudes. Dong et al. (2012) show that LSRTM can significantly improve image resolution and suppress migration artifacts.

In this study, we briefly review the theory and general workflow of LSRTM. Then we summarize its advantages and demonstrate the effectiveness for complex structure imaging via synthetic and real data examples. We also show that LSRTM is an affordable image-domain broadband solution that complements the deghosting technique for marine streamer data.

## Methodology

As a general least-squares inversion problem, LSRTM can be formulated as

$$m_{\text{mig}} = (L^T L)^{-1} L^T d_{\text{obs}}, \quad (1)$$

where  $m_{\text{mig}}$  is the migration image,  $L$  is the forward-modeling (demigration) operator, and  $d_{\text{obs}}$  represents the observed seismic data. For LSRTM,  $L^T$  is the RTM operator which is adjoint to the two-way modeling operator  $L$ . The inversion minimizes the following objective function in least-squares sense:

$$J(m) = \|p_m(Lm) - p_f d_{\text{obs}}\|, \quad (2)$$

where  $p_m$  is a filter applied to match the synthetic data to the observation preprocessed by operator  $p_f$ . Nemeth et al. (1999) derive the detailed equations for least-squares inversion based on the Kirchhoff method. For LSRTM, the inversion theory is the same except that the modeling and migration operators are based on RTM.

Figure 1 sketches the general workflow of LSRTM. First a conventional RTM image is used as the initial model of the inversion. Then synthetic data are generated by the two-way demigration operator (usually implemented via Born modeling). The waveforms of the input observations and the synthetic data are compared in time domain to generate residual gathers. Because of the adjoint relationship between the migration and demigration operators, reverse time propagation of the residuals generates the negative gradient for model updating. Convergence of the inversion refines the initial RTM image toward the true-reflectivity earth model.

One might notice that the LSRTM workflow is similar to that of FWI. The only difference is that in LSRTM, our model is a seismic image (reflectivity) rather than velocity. Thus we should assume that velocity is known perfectly for LSRTM. During the inversion, we use the seismic-wave velocity as a background parameter without any changes.

**Advantages of LSRTM**

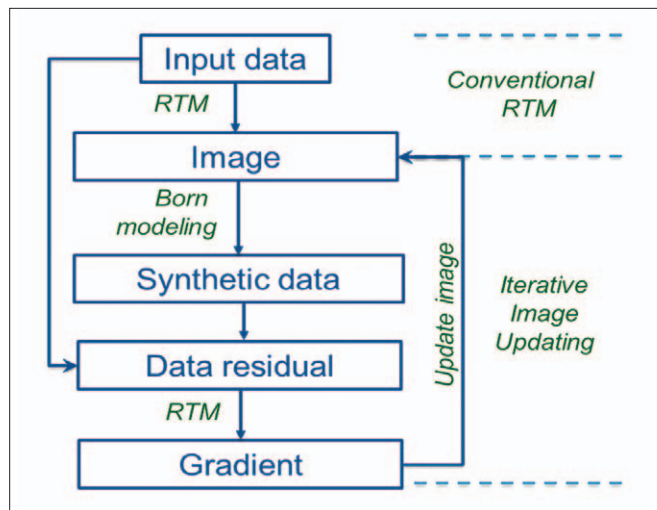
We demonstrate the potential advantages of LSRTM using two synthetic examples. We used a modified Marmousi model to create the first example. To simulate a deepwater environment, we extended the water depth of the original Marmousi model below 800 m. Then we ran finite-difference modeling using a 20-Hz (peak frequency) Ricker wavelet and moved the source and receivers to simulate a streamer acquisition. A total of 34 shots was used for migration and inversion.

Figure 2a displays the true (normal-incidence) reflectivities derived from the true Marmousi velocity model. Conventional RTM and LSRTM images after 20 iterations are shown in Figures 2b and 2c, respectively. Conventional RTM suffers from an uneven illumination problem (marked by the dashed ellipse) because of insufficient data.

In contrast, LSRTM creates an image whose amplitudes are more balanced and closer to the true-reflectivity model. Multiple iterations reduce migration swings. The image of the reservoir (marked by the arrow) is significantly improved. It is clear that the LSRTM image has much higher spatial resolution than conventional RTM by presenting sharper layer boundaries and blocky-looking 3D textures.

The image after LSRTM shows detailed stratigraphic information and geologic structures such as the valley and ridge province. The spectra comparison confirms the 3D broadband effect (Figure 2d) and demonstrates that the LSRTM image contains enriched low-frequency information that suppresses the side lobes of the image wavelets.

We create another synthetic example based on a real survey in the Gulf of Mexico (GOM). Figure 3a presents the true-reflectivity model that we want to retrieve. Two huge salt bodies that represent the typical salt-basin environment in the GOM dominate the model. A total of 190 shots is simulated via finite-difference acoustic modeling



**Figure 1.** General workflow of LSRTM. The first two modules belong to conventional RTM for the initial model, and the modules below compose the iteration part of LSRTM.

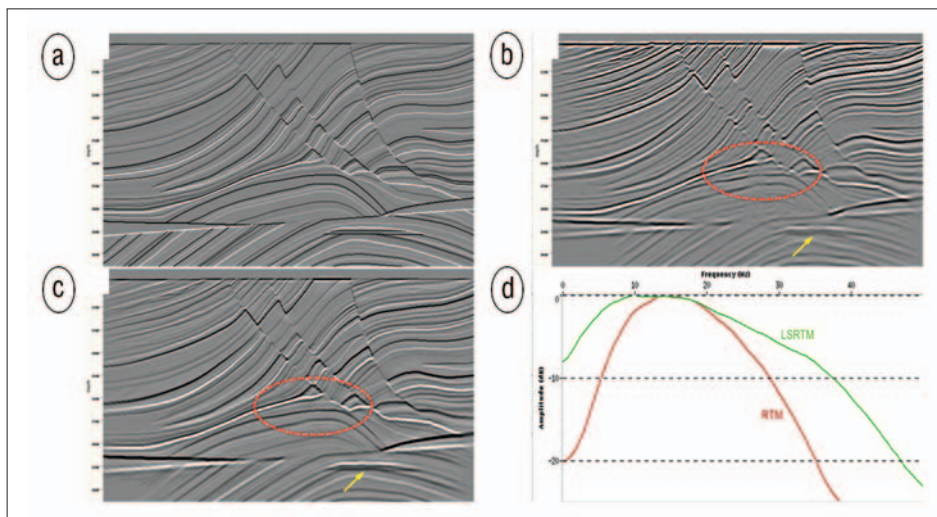


**Figure 2.** (a) True reflectivities, (b) conventional RTM image, and (c) LSRTM image of the modified Marmousi model. (d) Corresponding spectra comparison of the RTM and LSRTM images.

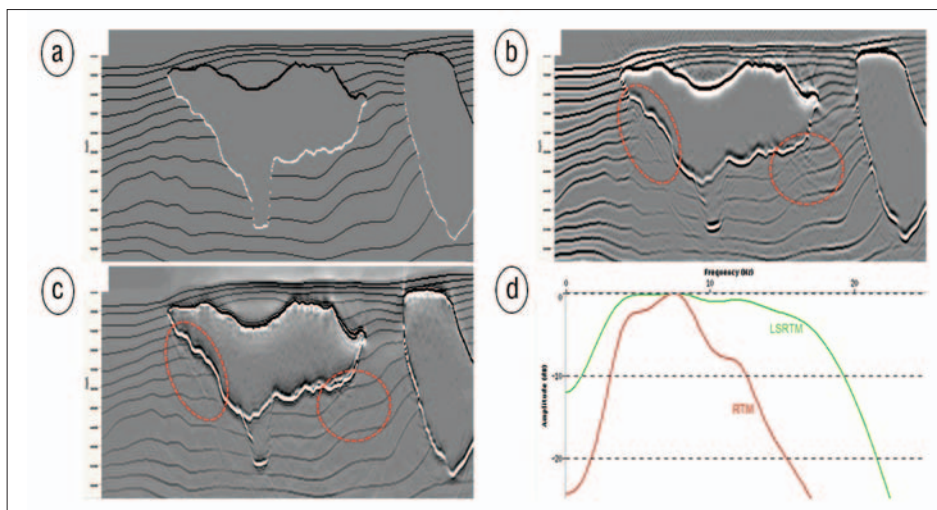


**Figure 3.** (a) True reflectivities, (b) conventional RTM image, and (c) LSRTM image of the salt model based on a Gulf of Mexico survey. (d) Corresponding spectra comparison of the RTM and LSRTM images.

Downloaded 09/10/14 to 205.196.179.238. Redistribution subject to SEG license or copyright; see Terms of Use at http://library.seg.org/

with a 6-km virtual towed-streamer cable. The corresponding RTM image is shown in Figure 3b, where migration artifacts appear near the major salt boundary. The image quality of the sediments near the left salt flank (marked by the dashed ellipse) is poor. In real surveys, this shadow zone is usually of great interest to interpreters because of the possible formation of reservoir traps.

With the illumination-compensation ability of LSRTM, the inverted result (Figure 3c) shows clearer structures around the salt flank, with reduced migration artifacts. On the lower right side of the major salt body (marked by the dashed circle), the strong swing noise on the original RTM image is suppressed after LSRTM.

By comparing the spatial spectra (Figure 3d) of the conventional RTM and the LSRTM images, it is evident that the LSRTM image poses a broader spectrum, which is closer to that of the true-reflectivity model (infinite-bandwidth white

spectrum). The extension of the spectrum increases the spatial resolution of the image, which greatly facilitates interpretation. The updated amplitudes of the image also approximate true-reflectivity values and are more physically plausible for extracting rock properties and for seismic-attribute analysis.

With these representative synthetic examples and the comparison with conventional RTM, we can summarize the advantages of LSRTM as follows:

- 1) Amplitudes are balanced better by revealing weak signals and pushing the image toward the true-reflectivity model.
- 2) Migration artifacts caused by acquisition footprints or nonuniform illumination are reduced.
- 3) Spatial resolution is increased by enriching the low frequencies and suppressing the image side lobes.
- 4) Signal-to-noise ratio is enhanced by improving the images of steep dips or other complex structures.

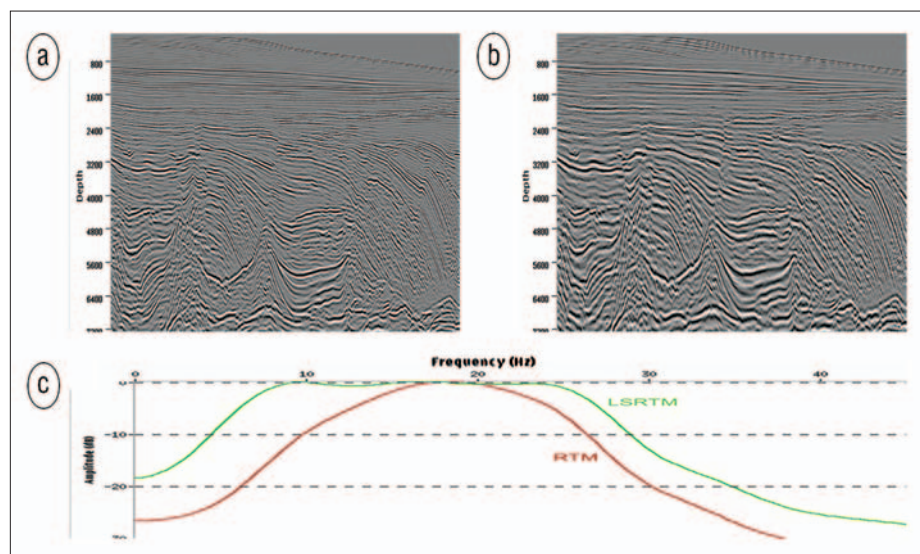


**Figure 4.** (a) Conventional RTM and (b) LSRTM images of line 1 of the 2D Brazil data with a major fault. (c) Corresponding spectra comparison of the RTM and LSRTM images.

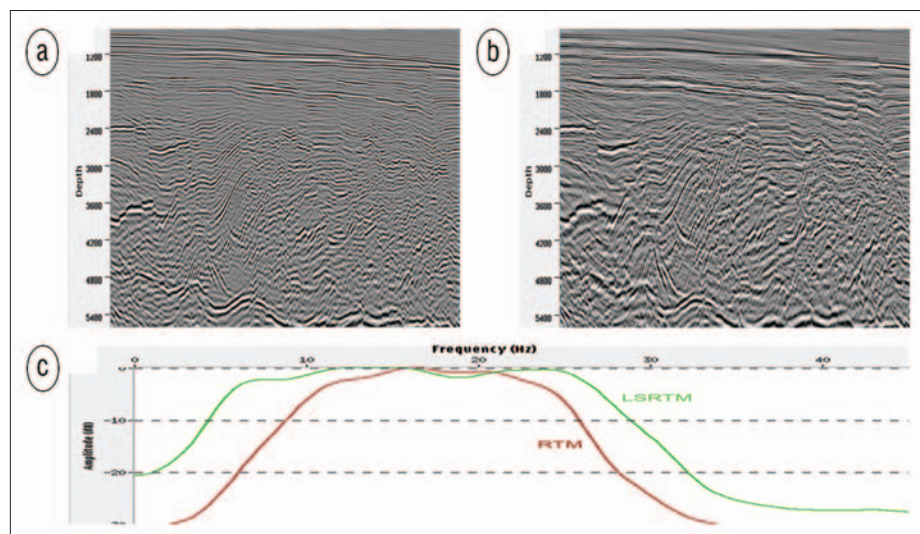


**Figure 5.** (a) Conventional RTM and (b) LSRTM images of line 2 of the 2D Brazil data with a large amount of fault groups. (c) Corresponding spectra comparison of the RTM and LSRTM images.

### Field data examples

In this section, we examine the effectiveness of LSRTM on field data. A 2D data set was acquired in Brazil using a 6-km streamer (data courtesy of the TGS/WesternGeco Brazil 2D Data Alliance). Figures 4a and 4b show the conventional anisotropic RTM and LSRTM images from one of the sail lines (line 1) in the area of interest, respectively. On the RTM image (Figure 4a), we can barely see a major fault in the center of the section. However, the accurate position of the fault plane is smeared because of insufficient reflection energy in the limited aperture.

This problem is resolved in LSRTM by enhancing the weak reflections and achieving better illumination compensation. On the LSRTM image (Figure 4b), the major fault is delineated clearly, with well-focused fault plane and sharp geologic termination. Similar to the synthetic tests, a 3D deconvolution effect results from suppression of the side lobes of the images.

Spectra analysis (Figure 4c) shows that LSRTM extends the spectrum toward low- and high-frequency ends and increases the octave range of the image for better spatial resolution.

Figure 5 illustrates the application of LSRTM to another section (line 2) of the 2D Brazil data. On the conventional RTM image (Figure 5a), the steeply dipping structures are imaged poorly because of

insufficient data coverage. In contrast, the LSRTM image (Figure 5b) clearly depicts the grabens by imaging the large amount of steeply dipping fault groups. Similar to the previous example, LSRTM recovered abundant frequencies on the image spectrum (Figure 5c) to greatly improve spatial resolution of the image and to facilitate detailed seismic interpretation.

### LSRTM for broadband imaging

Here we show a practical solution to create broadband images using LSRTM to overcome the high computational cost of RTM in the high-frequency band. Because LSRTM is an iterative inversion, it can use initial models that come from any migration algorithm in addition to RTM. In the following studies, we investigate an iterative LSRTM approach to integrate one-way wave-equation migration (WEM) and RTM methods for high-resolution broadband imaging.

We start from the high-frequency WEM image that is migrated from the deghosted input data and use it as the initial model for LSRTM. In the subsequent LSRTM iterations, we use a two-way wave equation for the demigration and migration computation to obtain full two-way gradients and recover the events on the WEM image that are missing because of angle limitations. Zeng et al. (2014) provide a more detailed explanation of this broadband LSRTM approach.

Figure 6 displays the conventional RTM image (Figure 6a), WEM image (Figure 6b), and broadband LSRTM image (Figure 6c) corresponding to a portion of the 2D Brazil data. The maximum frequencies for the RTM and WEM jobs are 25 Hz and 50 Hz, respectively. For the broadband LSRTM, we use the 50-Hz WEM image as the initial model but limit the maximum frequency to 25 Hz for the subsequent two-way iterations.

After several iterations, LSRTM presents a broadband image by enriching the low-frequency components and maintaining the high-frequency information. Compared with the original RTM image and the high-frequency WEM image, the steeply dipping faults are imaged significantly better, with focused fault planes and detailed sediments.

Based on the success of the broadband LSRTM on the 2D real data, we extend our study to 3D shallow-water streamer data from the Gulf of Mexico (data courtesy of TGS multient data library). Figure 7 compares the deghosted RTM image (Figure 7a) and the broadband LSRTM result (Figure 7b). Because of the broadband effect, the LSRTM image exhibits clearer fault planes and much higher-resolution horizons compared with those on the conventional deghosted RTM image.

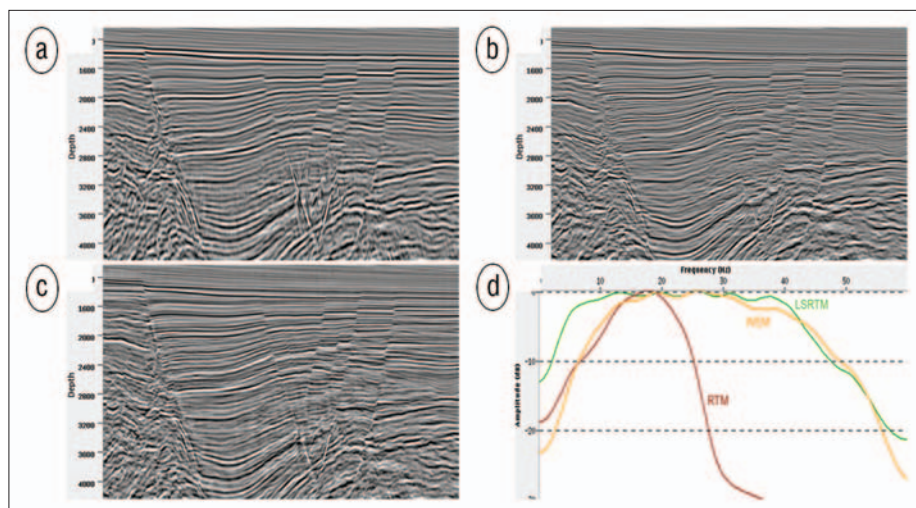


**Figure 6.** (a) Conventional RTM image, (b) deghosted high-frequency WEM image, and (c) broadband LSRTM image migrated from the 2D streamer data in Brazil. (d) Corresponding spectra. Red, orange, and green curves represent the normalized amplitude spectra of the RTM, WEM, and LSRTM images, respectively. Spectra are obtained via depth-to-time conversion.

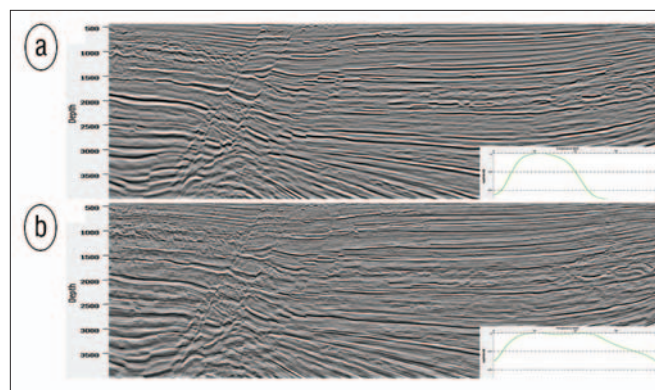


**Figure 7.** (a) Deghosted RTM image and (b) broadband LSRTM image migrated from the 3D streamer data in the Gulf of Mexico. Corresponding spectra are shown in the lower right corner of each image for comparison.

It is important to note that each iterative step of the broadband LSRTM takes about 3.5 hours for this 3D test. However, if we directly compute the 60-Hz RTM for the same model and data, the estimated total computation time is about 30 hours using exactly the same computing resources, disregarding the impractical GPU memory requirements. Therefore, the broadband LSRTM is more practically affordable than a direct high-frequency RTM.

### Conclusions

We briefly reviewed the theory and applications of LSRTM with synthetic and real data examples. As an inversion-based imaging algorithm, LSRTM inherits the advantages of conventional RTM as well as geophysical inversion. The iterative nature of LSRTM is the key to handling migration errors in conventional imaging. We demonstrated that LSRTM can create high-resolution and true-amplitude images by eliminating migration artifacts and pushing the image toward the true-reflectivity model. Compared with

conventional imaging that directly applies the imaging condition in a single step, LSRTM overcomes the shortcomings of conventional migration algorithms via iterative least-squares inversion. Side lobes of the image wavelets are suppressed in LSRTM to form images with high spatial resolution. Weak events are recovered, and steep dips are enhanced during iterations with balanced illumination.

The true-amplitude behavior of LSRTM will greatly benefit quantitative seismic interpretations. The least-squares inversion approach also can be used to integrate the advantages of different migration algorithms, and it provides a practical and affordable image-domain broadband solution to high-resolution imaging for complex structures. With the continued increase of computational power in the seismic industry, we believe that inversion-based imaging algorithms such as LSRTM will be the next-generation workhorse for seismic imaging. **TLE**

### References

- Dong, S., J. Cai, M. Guo, S. Suh, Z. Zhang, B. Wang, and Z. Li, 2012, Least-squares reverse time migration: Towards true amplitude imaging and improving the resolution: 82nd Annual International Meeting, SEG, Expanded Abstracts, <http://dx.doi.org/10.1190/segam2012-1488.1>.
- Dong, S., C. Zeng, H. Masoomzadeh, and B. Wang, 2014, Dehosted least-squares RTM — Image domain broadband solution for complex structures: 76th Conference and Exhibition, EAGE, Extended Abstracts, <http://dx.doi.org/10.3997/2214-4609.20141449>.
- Nemeth, T., C. Wu, and G. T. Schuster, 1999, Least-squares migration of incomplete reflection data: *Geophysics*, **64**, no. 1, 208–221, <http://dx.doi.org/10.1190/1.1444517>.
- Schuster, G. T., 1993, Least-squares cross-well migration: 63rd Annual International Meeting, SEG, Expanded Abstracts, 110–113, <http://dx.doi.org/10.1190/1.1822308>.
- Wang, B., S. Dong, and S. Suh, 2013, Practical aspects of least-squares reverse time migration: 75th Conference and Exhibition, EAGE, Extended Abstracts, <http://dx.doi.org/10.3997/2214-4609.20131000>.
- Zeng, C., S. Dong, J. Mao, and B. Wang, 2014, Broadband least-squares reverse time migration for complex structure imaging: 84th Annual International Meeting, SEG, Expanded Abstracts, 3715–3719, <http://dx.doi.org/10.1190/segam2014-1283.1>.

*Acknowledgments: The authors are grateful to Jean Ji, Davide Teixeira, Zhigang Zhang, Jian Mao, Sang Suh, Gary Rodriguez, and Zhiming Li for their great contributions and outstanding support of this research. They appreciate Connie VanSchuyver for manuscript assistance. They thank TGS management for permission to publish this article. The seismic data in 2D real-world examples are courtesy of TGS/WesternGeco Brazil 2D Data Alliance. The 3D seismic data in the Gulf of Mexico example are provided by the TGS multiclient data library.*

*Corresponding author: Chong.Zeng@tgs.com*